Physical and Thermal Studies of Carbon-Enriched Silicon Oxycarbide Synthesized from Floating Plants

Authors:

Guan-Ting Pan, Siewhui Chong, Yi Jing Chan, Timm Joyce Tiong, Jun Wei Lim, Chao-Ming Huang, Pradeep Shukla, Thomas Chung-Kuang Yang

Abstract:

In the present study, amorphous mesoporous silicon oxycarbide materials (SiOC) were successfully synthesized via a low-cost facile method by using potassium hydroxide activation, high temperature carbonization, and acid treatment. The precursors were obtained from floating plants (floating moss, water cabbage, and water caltrops). X-ray diffraction (XRD) results confirmed the amorphous Si?O?C structure and Raman spectra revealed the graphitized carbon phase. Floating moss sample resulted in a rather rough surface with irregular patches and water caltrops sample resulted in a highly porous network structure. The rough surface of the floating moss sample with greater particle size is caused by the high carbon/oxygen ratio (1: 0.29) and low amount of hydroxyl group compared to the other two samples. The pore volumes of these floating moss, water cabbage, and water caltrops samples were 0.4, 0.49, and 0.63 cm3 g?1, respectively, resulting in thermal conductivities of 6.55, 2.46, and 1.14 Wm?1 K?1, respectively. Floating plants, or more specifically, floating moss, are thus a potential material for SiOC production.

Article

Physical and Thermal Studies of Carbon-Enriched Silicon Oxycarbide Synthesized from Floating Plants

Guan-Ting Pan [1], Siewhui Chong [2], Yi Jing Chan [2], Timm Joyce Tiong [2], Jun Wei Lim [3], Chao-Ming Huang [4], Pradeep Shukla [5],* and Thomas Chung-Kuang Yang [1],*

[1] Department of Chemical Engineering and Biotechnology, National Taipei University of Technology, Taipei 106, Taiwan; gtpan@ntut.edu.tw
[2] Department of Chemical and Environmental Engineering, University of Nottingham Malaysia, Broga Road, Semenyih 43500, Malaysia; Faye.Chong@nottingham.edu.my (S.C.); Yi-Jing.Chan@nottingham.edu.my (Y.J.C.); Joyce.Tiong@nottingham.edu.my (T.J.T.)
[3] Department of Fundamental and Applied Sciences, Centre for Biofuel and Biochemical Research, Institute of Self-Sustainable Building, Universiti Teknologi PETRONAS, Seri Iskandar 32610, Malaysia; Junwei.lim@utp.edu.my
[4] Green Energy Technology Research Centre and Department of Materials Engineering, Kun Shan University, Tainan 710, Taiwan; charming@mail.ksu.edu.tw
[5] Queensland Alliance for Environmental Health Sciences, Faculty of Health and Behavioural Sciences, The University of Queensland, St Lucia, QLD 4072, Australia
* Correspondence: Pradeep.shula@uq.edu.au (P.S.); ckyang@mail.ntut.edu.tw (T.C.-K.Y.); Tel.: +61-7-336-56195 (P.S.); +886-2-2771-2171 (T.C.-K.Y.)

Abstract: In the present study, amorphous mesoporous silicon oxycarbide materials (SiOC) were successfully synthesized via a low-cost facile method by using potassium hydroxide activation, high temperature carbonization, and acid treatment. The precursors were obtained from floating plants (floating moss, water cabbage, and water caltrops). X-ray diffraction (XRD) results confirmed the amorphous Si–O–C structure and Raman spectra revealed the graphitized carbon phase. Floating moss sample resulted in a rather rough surface with irregular patches and water caltrops sample resulted in a highly porous network structure. The rough surface of the floating moss sample with greater particle size is caused by the high carbon/oxygen ratio (1: 0.29) and low amount of hydroxyl group compared to the other two samples. The pore volumes of these floating moss, water cabbage, and water caltrops samples were 0.4, 0.49, and 0.63 cm^3 g^{-1}, respectively, resulting in thermal conductivities of 6.55, 2.46, and 1.14 $Wm^{-1} K^{-1}$, respectively. Floating plants, or more specifically, floating moss, are thus a potential material for SiOC production.

Keywords: silicon oxycarbide; thermal conductivity; floating plants; SiOC; silica

1. Introduction

Silicon oxycarbide (SiOC) is an important material that finds application in semiconductor devices [1,2], electrode materials of lithium–ion batteries [3,4], micro electromechanical systems devices [5], high temperature sensors [6], conductive protective coatings [7], and super-capacitor [8] due to its superior mechanical properties. SiOC exhibits high strength [9], high chemical durability [10], excellent oxidation resistance under high temperature, good antioxidant crystallization property [11], and exceptional thermal expansion properties [12]. However, amongst these, thermal properties of silicon oxycarbide were rarely studied. Qiu et al. [13] reported a three-dimensional reticular macro-porous SiOC ceramic structure prepared by sol–gel process. The sample's porosity and specific surface area were reduced due to particle agglomeration, resulting in lower thermal conductivity that

ranged from 0.041 to 0.062 $Wm^{-1} K^{-1}$. Recently, random porous structure has attracted an increasing interest due to its radiation tolerance and very high crystallization temperature, which in turn resulted in good thermal conductivity [14,15]. Gurlo et al. [16] reported that the thermal conductivity of SiOC material containing zirconium and hafnium was 1.3 $Wm^{-1} K^{-1}$ which was similar to that of silica. Mazo et al. [17] observed that silicon oxycarbide glasses that were synthesized by using spark plasma sintering had higher thermal conductivity values ($\approx$1.38 $Wm^{-1} K^{-1}$). Eom, et al. [18] prepared barium-added silicon oxycarbide (SiOC–Ba) via pyrolysis method and showed that the addition of Ba resulted in an increase in thermal conductivity values from 1.8 to 5.6 $Wm^{-1} K^{-1}$.

The traditional approach to producing amorphous SiOC microstructure has been via physical and chemical processing methods, such as powder metallurgy process [19], magnetron sputtering [20], sol–gel method [21,22], and chemical vapor deposition [23]. The raw materials used in synthesizing these SiOC materials were mainly chemical feedstocks such as tetraethoxysilane (TEOS)/hydroxyl-terminated polydimethylsiloxane (PDMS) organic–inorganic hybrid materials [17], polyxiloxane [18], methyltrimethoxysilane and dimethyldimethoxysilane [22], and dimethyl dimethoxy silane [21]. There are also limited studies on the thermal conductivity of SiOC materials. It could be expected that the material's structure affects its heat transfer properties as the type of particles and different pore sizes in the SiOC structure are the main reason to the different thermal conductivity abilities [12]. Low-cost sacrificial template has been widely used to generate replicated pore structures within such ceramic materials. Utilizing organic bio-mass, such as wood, or chemically modified biomass as a template for synthesizing SiOC with varying degree of porosity has been reported [24,25]. The use of selected biomass can also provide an added advantage of providing a source of silica for synthesis of SiOC.

These observations motivated our research for synthesizing SiOC using plant based biomass and to evaluate its physical properties and thermal conductivity. The main advantages of this method, as compared to other technologies, are its benign environmental nature and production of high-purity products via a low-cost process. In this study, silicon oxycarbide materials were synthesized by using a facile and inexpensive route from floating plants (floating moss, water cabbage, and water caltrops). The characterizations of these silicon oxycarbide materials were studied with regards to their structural, morphology, functional group, textural properties, and thermal conductivity.

2. Experimental

2.1. Preparation of Materials

All chemicals of analytical grade were purchased from Merck Chemicals. Three floating plants were used to synthesize carbon-enriched silicon oxycarbide (SiOC), namely, floating moss (Salvinia natans), water cabbage (Pistia stratiotes), and water caltrops (Trapa natans). The plants were collected from a pond at Kun Shan University, Tainan, Taiwan. The plants were washed and bone-dried in an oven at 100 °C before being grinded using a blender. For each sample synthesis, 0.071 mole potassium hydroxide (KOH) was dissolved in 40 mL of deionized water into which 1 gram of the dried and grounded biomass was added. The mixture was stirred for 2 h at 85 °C for activation before being annealed for 2 h in a tube furnace purged with nitrogen gas at 800 °C for carbonization. After that, the samples were added into 1.8 M hydrochloric acid (HCl) under magnetic stirring for 1 h. The resultant solid powder from the mixture solutions were washed by vacuum filtration until the pH value reached 7, and finally dried in vacuum at 110 °C overnight. The KOH activation enlarged the pores in these samples, thereby destroying their internal structure. These carbon-rich materials were then converted into pure carbon via high-temperature carbonization. Finally, acidic treatment (HCl) was used to alter the surface functional groups, surface morphology, and textural properties of the samples.

2.2. Characterization of Carbon-Enriched Silicon Oxycarbide

The crystalline structures of the carbon-enriched silicon oxycarbide samples were studied using an X-ray diffractometer (PANalytical X'Pert PRO, Almelo, the Netherlands) with copper K–alpha radiation ($\lambda = 0.15418$ nm) scanning from 10° to 70°. The structures of all samples were analyzed using Raman Spectroscopy (DONGWOO DM500i, Gyeonggi-do, Korea). The morphology and compositions of the SiOC samples were analyzed via a field emission scanning electron microscopy (FESEM, JEOL JSM-6700F, JEOL, Peabody, MA, USA) with energy-dispersive X-ray spectroscopy (EDX). The morphology imaging was carried out at 5 k magnification with an accelerating voltage of 12 kV and a working distance of 12.1 mm. TEM observations of precipitates were performed on selected samples, using a transmission electron microscopy (TEM, JEM2100F, Akishima, Japan) at 200 kV. Fourier transform infrared (FTIR) spectroscopy (Perkin Elmer Spectrum GX, Shelton, CT, USA) was carried out to study the sample's structure using a diffuse reflectance infrared Fourier transform accessory (DRIFT) equipped with a heating cartridge. The pore textural characterizations of the samples were measured by a volumetric sorption analyzer (Micromeritics ASAP 2020, Micromeritics Instrument Corporation, Norcross, GA, USA). An adsorption/desorption isotherm of nitrogen gas was recorded at −196 °C and the pore size distribution was investigated by using the Barrett–Joyner–Halenda (BJH) model for the specific surface area and pore volume of the samples. The thermal conductivity absolute value was directly determined by a thermal conductivity probe (Mathis Instruments Ltd., Fredericton, Canada).

3. Results and Discussion

3.1. Structural Analysis

XRD patterns of the SiOC samples are shown in Figure 1. The patterns correspond to an amorphous Si–O–C material feature with disordered carbon and with broad (002) and (100) at 2θ angles of 22.5° and 44°, respectively [26,27]. The peak at 44° is involved with small graphene sheets, and the peak at 22.5° means small graphene sheets stacked with random rotations or translations [27]. Raman spectra are also provided in Figure 2 for comparison. The Raman spectra of the prepared samples show the presence of two peaks at 1350 and 1582 cm^{-1}, corresponding to D- and G-bands. The relative intensity/area ratio of D- and G-bands can be used to analyze the carbon material's structure. The G-band is a reflection of the presence of sp2 carbon–carbon bond hybridization within a graphitic ring structure, whereas the D band reflect a disordered carbon structure. It can be seen that the G band of these samples is broader than the D band, indicating the high graphitized carbon structure in these samples [28,29].
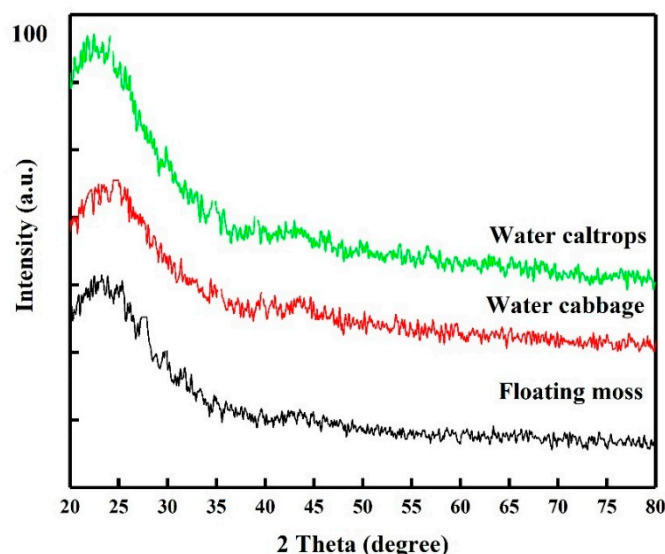

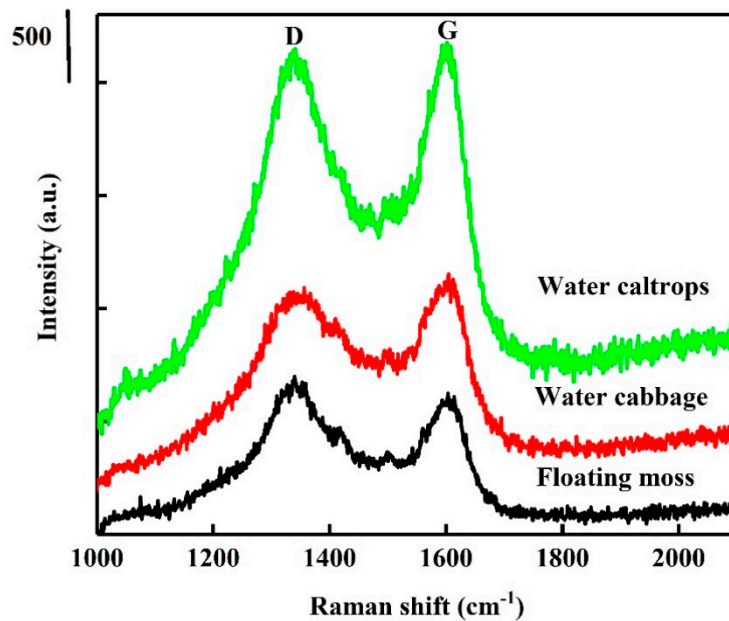**Figure 1.** X-ray diffraction patterns of the silicon oxycarbide (SiOC) samples.

Figure 2. Raman spectra of the silicon oxycarbide (SiOC) samples.

3.2. Morphology and Composition Analysis

Figure 3 shows the field emission scanning electron microscopy (FESEM), TEM images, and EDX spectra of the prepared samples. Figure 3a shows that the floating mass sample contains a rough surface with irregular patches. Figure 3b, on the other hand, shows that the water cabbage sample contains a randomly distributed and overlapped structure. Contradictorily, Figure 3c shows an interconnected three-dimensional layered material for the water caltrops sample. Apart from the overall view by FESEM, all TEM images showed that these samples contained ordered hexagonal pore arrays with the majority of pores less than 1 nm.

The quantitative analysis was carried out with using energy dispersion analysis to determine the atomic ratios of C, O, and Si in these samples. As shown in Figure 3, the samples contain no contaminations other than C, O, and Si elements. Table 1 shows that the atomic ratios of C, O, and Si of the samples are 1:0.29:0.06, 1:1.13:0.48, and 1:2.24:1.07, respectively for the floating moss, water cabbage, and water caltrops samples. It is apparent that the element oxygen plays an important role to form structural layering. The surface roughness of the samples reduces with a decrease in the ratio of carbon/oxygen. The respective layers of water caltrops sample display a parallel arrangement due to the low ratio of carbon/oxygen. Shen et al. [30] reported that the surface structure becomes rougher when there is a deprivation of epoxide and hydroxyl groups, as well as a high C/O ratio.
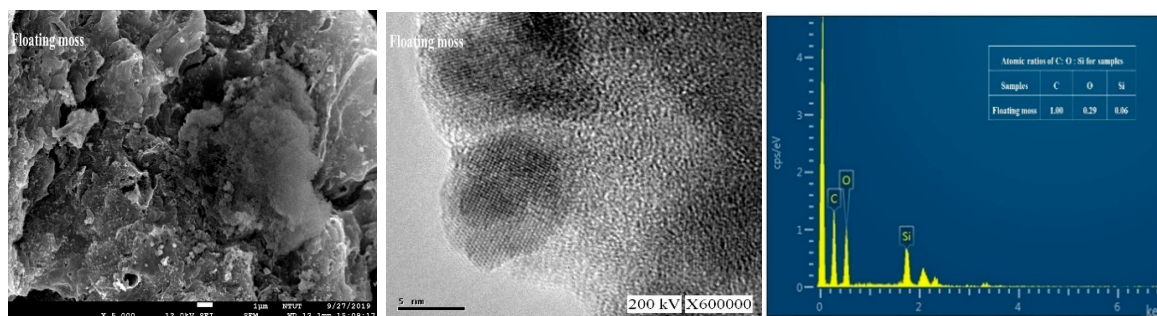
(**a**)

Figure 3. *Cont.*
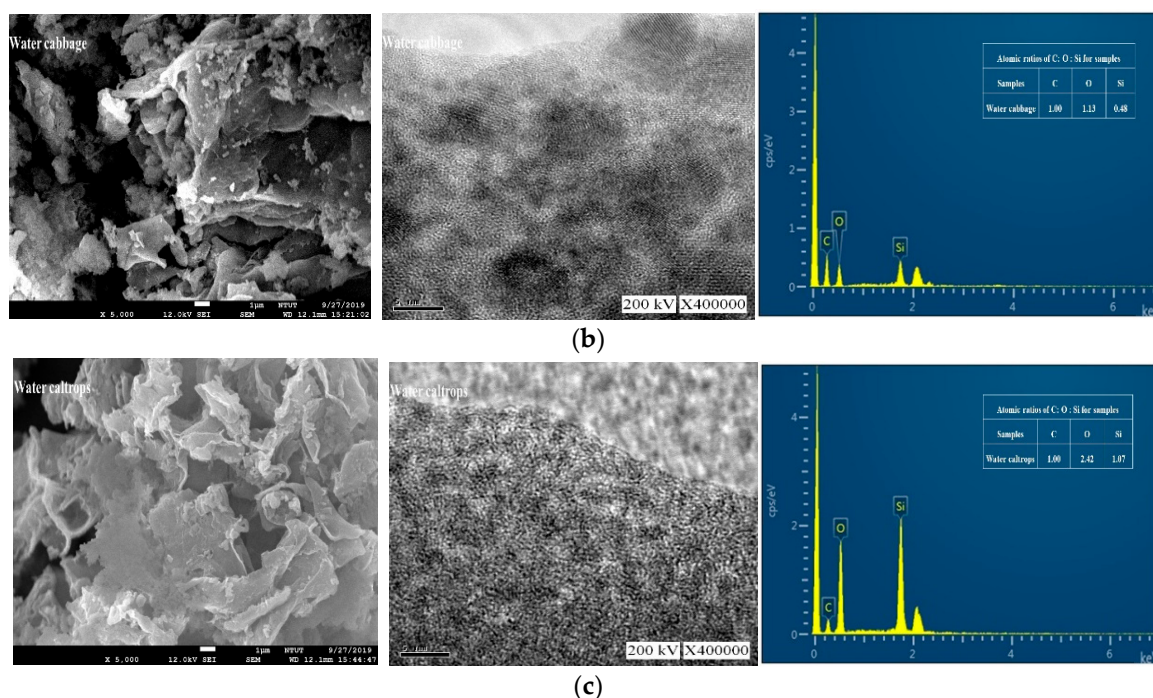
Figure 3. Field emission scanning electron microscopy (FESEM), transmission electron microscopy (TEM) and energy-dispersive X-ray spectroscopy (EDX) images (from left to right) of (**a**) Floating moss sample; (**b**) Water cabbage sample; and (**c**) Water caltrops sample.

Table 1. The C, O, and Si contents of the samples obtained by energy-dispersive X-ray spectroscopy (EDX) analysis.

	Atomic Ratios		
Sample	**C**	**O**	**Si**
Floating moss	1	0.29	0.06
Water cabbage	1	1.13	0.48
Water caltrops	1	2.42	1.07

3.3. Fourier Transform Infrared Spectroscopy (FTIR) Spectra

Figure 4 shows the FTIR spectra of the SiOC samples. Before the IR spectra analysis, the adsorbed water was removed by heating to 250 °C to advance the understanding of the functional group properties. The stretching vibration of siloxane bond (Si–O–Si) and the Si–O stretching vibration of the silanol group appear weak at 800 cm^{-1} and 972 cm^{-1}, individually [31,32]. The asymmetric vibration of the Si–O–Si obviously appears at 1100 cm^{-1} [33] for water cabbage and water caltrops samples. However, in the floating moss sample, the Si–O–Si asymmetric vibration sharply reduces, due to the low amount of O and Si present in the structure. In addition, the floating moss sample has the lowest amount of hydroxyl groups, indicated by the low peak at 3450 cm^{-1}. The water caltrops sample has the highest amount of hydroxyl groups. The amount of hydroxyl groups corresponds to the particle size from FESEM morphology in which the floating moss sample with the lowest amount of hydroxyl groups has a larger particle size compared to the water cabbage and water caltrops samples. It is speculated that the particle size of the floating moss sample is larger as the hydroxyl groups of the sample may generate some surface charge, thus resulting in agglomeration [34].
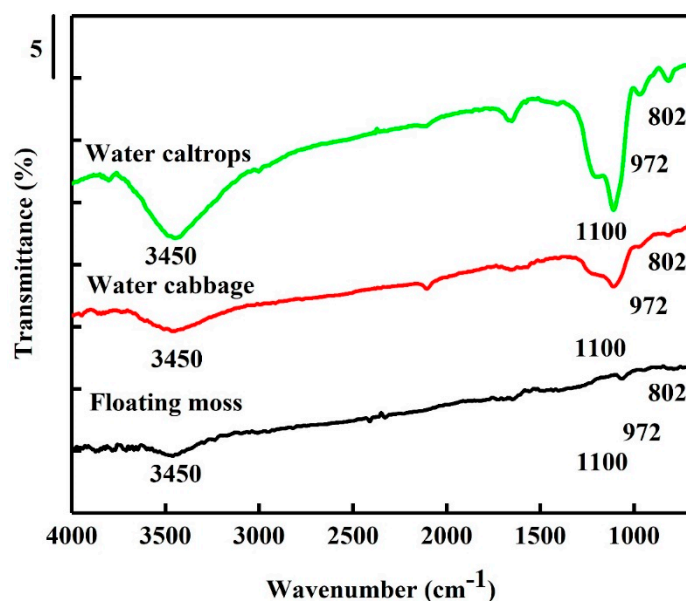
Figure 4. Fourier transform infrared (FTIR) spectra of the silicon oxycarbide (SiOC) samples.

3.4. Porosity and Surface Area Study

Figure 5a shows the nitrogen adsorption–desorption isotherms of the prepared samples. There is a very slow increase in N_2 adsorption up to 0.80 of the relative pressure (P/P_0) before the sharp rise in the adsorbed volume when capillary condensation occurred. A H_2-type hysteresis loop consisting of a triangular shape and a steep desorption branch of the isotherms can be found, indicating the existence of highly meso-pores with narrow mouths and wider bodies (ink-bottle pores) [35]. Figure 5b shows the corresponding pore size distributions of the prepared samples. There is a narrow pore size distribution centered at around 2.75 nm with a small meso-pore part in the floating moss sample and water cabbage sample. In addition, the water caltrops sample has the most porous structures with pore diameters ranged from 4 to 32 nm, indicating that it belongs to hierarchical porous structure. Table 2 shows the specific surface area, pore volume, and average pore diameter calculated using the Barrett–Joyner–Halenda (BJH) equation.
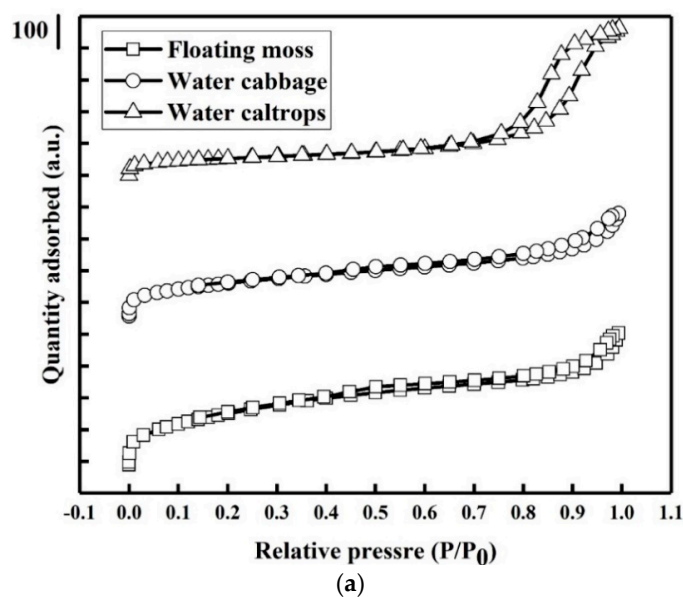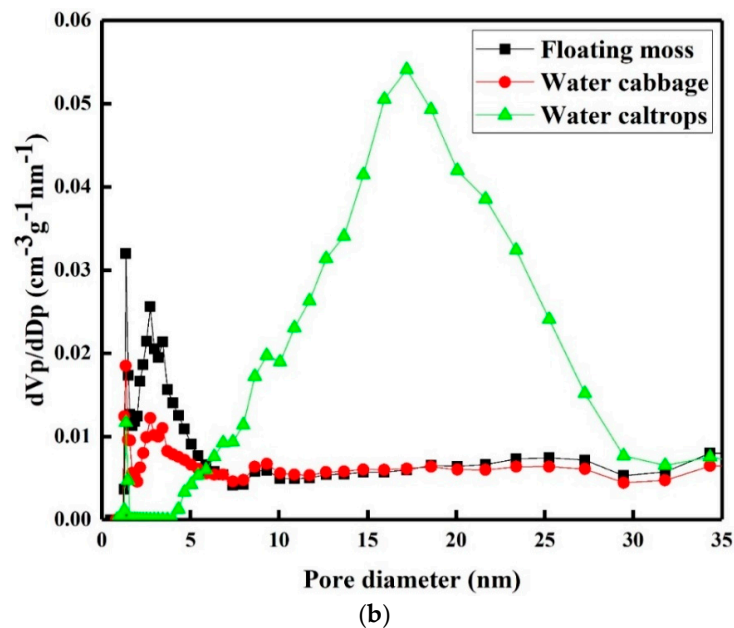

(a)

Figure 5. *Cont.*

Figure 5. (**a**) Nitrogen adsorption/desorption isotherms and (**b**) pore size distributions of the silicon oxycarbide (SiOC) samples.

Table 2. Textural characterization for the silicon oxycarbide (SiOC) samples.

Sample	V_{pore} $(cm^3\ g^{-1})$	S_{BET} $(m^2\ g^{-1})$	D_P (nm)	Thermal Conductivity $(Wm^{-1}\ K^{-1})$
Floating moss	0.40	894.81	7.00	6.55
Water cabbage	0.49	565.21	6.04	2.46
Water caltrops	0.63	213.00	4.75	1.14

The pore volumes (V_{pore}) of the floating moss, water cabbage, and water caltrops samples are respectively 0.4, 0.49, and 0.63 $cm^3\ g^{-1}$. The Brunauer–Emmett–Teller (BET) specific surface areas (S_{BET}) of the floating moss sample is greater than the water cabbage and water caltrops samples. The BJH adsorption-average pore diameters (D_p) are 7.00, 6.04, and 4.75 nm, respectively, for the floating moss, water cabbage, and water caltrops samples. The texture properties of the prepared samples agree with the surface morphology results in which the floating moss sample having the largest grain size has the lowest pore volume and largest pore diameter.

3.5. Thermal Conductivity

The thermal conductivities of these samples were studied using Yang et al.'s method [36]. The thermal conductivities of these samples are shown in Table 2 and compared with other literature in Table 3. As we can see, the thermal conductivity of the floating moss sample is the highest among these samples due to lowest pore volume and larger grain size [12]. The water caltrops sample has the lowest thermal conductivity among these samples, indicating that the surface hydroxyl groups on silica reduced the thermal conductivity of the sample due to the increased amount of voids [37]. Eom et al. [38] also reported that the equivalent porosity is the reason for low thermal conductivity. Thermal conductivity of these SiOC samples reduces in the order of floating moss (6.55 $Wm^{-1}\ K^{-1}$), water cabbage (2.46 $Wm^{-1}\ K^{-1}$), and water caltrops (1.14 $Wm^{-1}\ K^{-1}$). However, when compared with other literature (Table 3), the thermal conductivity of our floating-plant derived SiOC samples is considerably higher and comparable with those made from chemical feedstock. It is also a key finding that the surface hydroxyl groups on silica decreases the thermal conductivity. Nevertheless, among the

three floating plants: floating moss, water cabbage, and water caltrops, the floating mass plant is the candidate with the most potential to replace the use of chemical precursors in making SiOC.

Table 3. Comparison of thermal conductivity with other literature.

No	Precursors	Method	Thermal Conductivity $(Wm^{-1} K^{-1})$	References
1	Silicon oxide carbide powders	Pyrolysis	1.8~2.7	[12]
2	Alkoxy silane	Sol–gel	0.041~0.078	[13]
3	Polysiloxane pyrolysis residue, and barium isopropoxide	Pyrolysis	1.8~5.6	[18]
4	Commercial poly(methylsilsesquioxane) starting polymer and zirconium acetylacetonate	Pyrolysis	2	[16]
5	Silicon oxycarbide (SiOC) powders	Spark plasma sintering	1.38	[17]
6	Floating plants	Pyrolysis	1.14~6.55	This paper

4. Conclusions

In this study, silicon oxycarbide materials were synthesized via a simple and low-cost method from floating plants. Three floating plants: floating moss, water cabbage, and water caltrops were used as the precursors of the SiOC powders. XRD shows the amorphous Si–O–C material structure as the major phase. The morphologies and textural properties of the SiOC samples were porous micro-structures. The maximum thermal conductivity of the prepared samples in this study was found to be 6.55 $Wm^{-1} K^{-1}$ from floating moss. The surface hydroxyl groups of the SiOC samples may have possibly reacted with the silica atom, resulting in interconnecting bonds and thus larger grain size which enhances the thermal conductivity. Overall, the results demonstrated the feasibility of using floating plants as the precursor in making SiOC powder with high thermal conductivity via a facile and low-cost procedure, making it a suitable process for industrial applications.

Author Contributions: Conceptualization and writing, G.-T.P.; Review, S.C.; Validation, Y.J.C.; Sample analysis, T.J.T.; Funding acquisition, J.W.L.; Resources, C.-M.H.; Editing and finalization, P.S.; Supervision, T.C.-K.Y.

Conflicts of Interest: The authors declare no conflicts of interest.

References

1. Miyajima, H.; Masuda, H.; Watanabe, K.; Ishikawa, K.; Sekine, M.; Hori, M. Chemical bonding structure in porous SiOC films (k < 2.4) with high plasma-induced damage resistance. *Micro Nano Eng.* **2019**, *3*, 1–6.
2. Colombo, P.; Mera, G.; Riedel, R.; Soraru, G.D. Polymer-derived ceramics: 40 years of research and innovation in advanced ceramics. *J. Am. Ceram. Soc.* **2010**, *93*, 1805–1837. [CrossRef]
3. Wu, Z.; Lv, W.; Cheng, X.; Gao, J.; Qian, Z.; Tian, D.; Li, J.; He, W.; Yang, C. A Nanostructured Si/SiOC Composite Anode with Volume-Change-Buffering Microstructure for Lithium-Ion Batteries. *Chem. A Eur. J.* **2019**, *25*, 2604–2609. [CrossRef]
4. Wu, Z.; Cheng, X.; Tian, D.; Gao, T.; He, W.; Yang, C. SiOC nanolayers directly-embedded in graphite as stable anode for high-rate lithium ion batteries. *Chem. Eng. J.* **2019**, *375*, 121997. [CrossRef]
5. Duan, L.; Ma, Q.; Mei, L.; Chen, Z. Fabrication and electrochemical performance of nanoporous carbon derived from silicon oxycarbide. *Microporous Mesoporous Mater.* **2015**, *202*, 97–105. [CrossRef]
6. Roth, F.; Schmerbauch, C.; Ionescu, E.; Nicoloso, N.; Guillon, O.; Riedel, R. High-temperature piezoresistive C/SiOC sensors. *J. Sens. Sens. Syst.* **2015**, *4*, 133–136. [CrossRef]

7. Bik, M.; Stygar, M.; Jeleń, P.; Dąbrowa, J.; Leśniak, M.; Brylewski, T.; Sitarz, M. Protective-conducting coatings based on black glasses (SiOC) for application in solid oxide fuel cells. *Int. J. Hydrogen Energy* **2017**, *42*, 27298–27307. [CrossRef]

8. Tolosa, A.; Krüner, B.; Jäckel, N.; Aslan, M.; Vakifahmetoglu, C.; Presser, V. Electrospinning and electrospraying of silicon oxycarbide-derived nanoporous carbon for supercapacitor electrodes. *J. Power Source* **2016**, *313*, 178–188. [CrossRef]

9. Wu, N.; Wang, B.; Wang, Y. Enhanced mechanical properties of amorphous Si OC nanofibrous membrane through in situ embedding nanoparticles. *J. Am. Ceram. Soc.* **2018**, *101*, 4763–4772. [CrossRef]

10. Sorarù, G.D.; Modena, S.; Guadagnino, E.; Colombo, P.; Egan, J.; Pantano, C. Chemical durability of silicon oxycarbide glasses. *J. Am. Ceram. Soc.* **2002**, *85*, 1529–1536. [CrossRef]

11. Saha, A.; Raj, R. Crystallization maps for SiCO amorphous ceramics. *J. Am. Ceram. Soc.* **2007**, *90*, 578–583. [CrossRef]

12. Stabler, C.; Reitz, A.; Stein, P.; Albert, B.; Riedel, R.; Ionescu, E. Thermal properties of SiOC glasses and glass ceramics at elevated temperatures. *Materials* **2018**, *11*, 279. [CrossRef] [PubMed]

13. Qiu, L.; Li, Y.; Zheng, X.; Zhu, J.; Tang, D.; Wu, J.; Xu, C. Thermal-conductivity studies of macro-porous polymer-derived SiOC ceramics. *Int. J. Thermophys.* **2014**, *35*, 76–89. [CrossRef]

14. Santana, J.A.C.; Mora, E.E.; Price, L.; Balerio, R.; Shao, L.; Nastasi, M. Synthesis, thermal stability and the effects of ion irradiation in amorphous Si–O–C alloys. *Nucl. Instrum. Methods Phys. Res. Sect. B Beam Interact. Mater. At.* **2015**, *350*, 6–13. [CrossRef]

15. Nastasi, M.; Su, Q.; Price, L.; Santana, J.A.C.; Chen, T.; Balerio, R.; Shao, L. Superior radiation tolerant materials: Amorphous silicon oxycarbide. *J. Nucl. Mater.* **2015**, *461*, 200–205. [CrossRef]

16. Gurlo, A.; Ionescu, E.; Riedel, R.; Clarke, D.R. The Thermal Conductivity of Polymer-Derived Amorphous Si–O–C Compounds and Nano-Composites. *J. Am. Ceram. Soc.* **2016**, *99*, 281–285. [CrossRef]

17. Mazo, M.A.; Palencia, C.; Nistal, A.; Rubio, F.; Rubio, J.; Oteo, J.L. Dense bulk silicon oxycarbide glasses obtained by spark plasma sintering. *J. Eur. Ceram. Soc.* **2012**, *32*, 3369–3378. [CrossRef]

18. Eom, J.-H.; Kim, Y.-W.; Kim, K.J.; Seo, W.-S. Improved electrical and thermal conductivities of polysiloxane-derived silicon oxycarbide ceramics by barium addition. *J. Eur. Ceram. Soc.* **2018**, *38*, 487–493. [CrossRef]

19. Yan, X.; Wang, F.; Hattar, K.; Nastasi, M.; Cui, B. Novel amorphous SiOC dispersion-strengthened austenitic steels. *Materialia* **2019**, *6*, 100345. [CrossRef]

20. Zare, A.; Su, Q.; Gigax, J.; Shojaee, S.; Harriman, T.; Nastasi, M.; Shao, L.; Materer, N.; Lucca, D. Effects of ion irradiation on chemical and mechanical properties of magnetron sputtered amorphous SiOC. *Nucl. Instrum. Methods Phys. Res. Sect. B Beam Interact. Mater. At.* **2019**, *446*, 10–14. [CrossRef]

21. Zare, M.; Niroumand, B.; Maleki, A.; Allafchian, A.R. Sol-gel synthesis of amorphous SiOC nanoparticles from BS290 silicone precursor. *Ceram. Int.* **2017**, *43*, 12898–12903. [CrossRef]

22. Liu, C.; Meng, X.; Zhang, X.; Hong, C.; Han, J.; Han, W.; Xu, B.; Dong, S.; Du, S. High temperature structure evolution of macroporous SiOC ceramics prepared by a sol–gel method. *Ceram. Int.* **2015**, *41*, 11091–11096. [CrossRef]

23. Yu, S.; Tu, R.; Goto, T. Preparation of SiOC nanocomposite films by laser chemical vapor deposition. *J. Eur. Ceram. Soc.* **2016**, *36*, 403–409. [CrossRef]

24. Zollfrank, C.; Kladny, R.; Sieber, H.; Greil, P. Biomorphous SiOC/C-ceramic composites from chemically modified wood templates. *J. Eur. Ceram. Soc.* **2004**, *24*, 479–487. [CrossRef]

25. Pan, J.; Pan, J.; Cheng, X.; Yan, X.; Lu, Q.; Zhang, C. Synthesis of hierarchical porous silicon oxycarbide ceramics from preceramic polymer and wood biomass composites. *J. Eur. Ceram. Soc.* **2014**, *34*, 249–256. [CrossRef]

26. Wang, M.; Xia, Y.; Wang, X.; Xiao, Y.; Liu, R.; Wu, Q.; Qiu, B.; Metwalli, E.; Xia, S.; Yao, Y. Silicon oxycarbide/carbon nanohybrids with tiny silicon oxycarbide particles embedded in free carbon matrix based on photoactive dental methacrylates. *ACS Appl. Mater. Interfaces* **2016**, *8*, 13982–13992. [CrossRef]

27. Xue, J.; Myrtle, K.; Dahn, J. An Epoxy-Silane Approach to Prepare Anode Materials for Rechargeable Lithium Ion Batteries. *J. Electrochem. Soc.* **1995**, *142*, 2927–2935. [CrossRef]

28. Dibandjo, P.; Graczyk-Zajac, M.; Riedel, R.; Pradeep, V.; Soraru, G. Lithium insertion into dense and porous carbon-rich polymer-derived SiOC ceramics. *J. Eur. Ceram. Soc.* **2012**, *32*, 2495–2503. [CrossRef]

29. Fukui, H.; Ohsuka, H.; Hino, T.; Kanamura, K. A Si–O–C composite anode: High capability and proposed mechanism of lithium storage associated with microstructural characteristics. *ACS Appl. Mater. Interfaces* **2010**, *2*, 998–1008. [CrossRef]

30. Shen, L.; Zhang, L.; Wang, K.; Miao, L.; Lan, Q.; Jiang, K.; Lu, H.; Li, M.; Li, Y.; Shen, B. Analysis of oxidation degree of graphite oxide and chemical structure of corresponding reduced graphite oxide by selecting different-sized original graphite. *RSC Adv.* **2018**, *8*, 17209–17217. [CrossRef]

31. Amutha, K.; Ravibaskar, R.; Sivakumar, G. Extraction, synthesis and characterization of nanosilica from rice husk ash. *Int. J. Nanotechnol. Appl.* **2010**, *4*, 61–66.

32. Witoon, T.; Chareonpanich, M.; Limtrakul, J. Synthesis of bimodal porous silica from rice husk ash via sol–gel process using chitosan as template. *Mater. Lett.* **2008**, *62*, 1476–1479. [CrossRef]

33. Rida, M.A.; Harb, F. Synthesis and characterization of amorphous silica nanoparitcles from aqueous silicates uisng cationic surfactants. *J. Met. Mater. Miner.* **2014**, *24*, 37–42.

34. Chapter 3 Surface chemistry of porous silica. *J. Chromatogr. Libr.* **1979**, *16*, 57–146. [CrossRef]

35. Kruk, M.; Jaroniec, M. Gas adsorption characterization of ordered organic–Inorganic nanocomposite materials. *Chem. Mater.* **2001**, *13*, 3169–3183. [CrossRef]

36. Yao, W.; Guangsheng, G.; Fei, W.; Jun, W. Fluidization and agglomerate structure of SiO_2 nanoparticles. *Powder Technol.* **2002**, *124*, 152–159. [CrossRef]

37. Pan, G.-T.; Chong, S.; Yang, T.C.-K.; Yang, Y.-L.; Arjun, N. Surface modification of amorphous SiO_2 nanoparticles by oxygen-plasma and nitrogen-plasma treatments. *Chem. Eng. Commun.* **2016**, *203*, 1666–1670. [CrossRef]

38. Eom, J.-H.; Kim, Y.-W.; Raju, S. Processing and properties of macroporous silicon carbide ceramics: A review. *J. Asian Ceram. Soc.* **2013**, *1*, 220–242. [CrossRef]